Experimental sandbox tracer tests to characterize a binary aquifer via an Ensemble Kalman filter method

Valeria Todaro; Marco D'Oria; Andrea Zanini; J. Jaime Gómez-Hernández; Maria Giovanna Tanda

Abstract

Estimating the aquifer properties and their spatial variability is the most challenging part of groundwater flow and transport simulations. In this work, an ensemble Kalman-based method, the ES-MDA, is applied to infer the characteristics of a binary field by means of a tracer test reproduced in an experimental sandbox. Two different approaches are compared: the first one aims at estimating the hydraulic conductivity over the whole field assuming that the rest of the hydraulic and transport parameters are known by applying the standard ES-MDA method; the second one couples the ES-MDA with a truncated Gaussian model to simultaneously estimate the spatial distribution of two geological lithotypes and their main hydraulic and transport properties. Both procedures are tested following a fully-parameterized approach and a pilot point approach. A synthetic case that mimics the sandbox experiment was developed to test the capability of the proposed methods and find out their optimal configurations to be used for the real case. The results show that the ES-MDA coupled with a truncated Gaussian model outperforms the standard ES-MDA and it reproduces well the binary field and the aquifer properties also in presence of large measurement errors. The fully parametrized and pilot points approach lead to comparable solutions, with less computation time required by the pilot point approach.

1. Introduction

Aquifer characterization is fundamental for developing effective engineering strategies and applications, such as the planning of groundwater extraction or recharge systems and the assessment of the spatiotemporal evolution of subsurface contaminants. However, the identification of aquifer hydraulic and transport properties is still a subject under investigation in the scientific community. Many of these parameters cannot be estimated directly and need to be inferred through inverse modelling. Several approaches have been developed to address the inverse problem; extensive reviews have been carried out by Zimmerman et al. (1998), Vrugt et al. (2008) and Zhou et al. (2014).

In the past years, ensemble Kalman filter-based methods gained increasing interest due to their efficiency and flexibility in data assimilation for large nonlinear models. In fact, aquifer characterization by inverse modelling using gradient-based optimization approaches needs massive computational efforts for moderately large systems. The ensemble Kalman filter-based methods saves considerable computing time and does not need to resort to, for instance, pilot point techniques and variogram-based interpolations, commonly used in full Bayesian approaches, to reduce the number of unknown parameters. Hendricks Franssen and Kinzelbach (2009) compared the Ensemble Kalman filter (EnKF) with a Monte-Carlo type inverse modelling technique, the sequential self-calibration method, for inverse modelling of groundwater flow systems. The two methods give similar results; however, the EnKF computational cost is 80 times lower than that required by the sequential self-calibration method.

Since the introduction of the Ensemble Kalman filter (EnKF) by Evensen (1994), it has been widely used for data assimilation and inverse modelling in several fields, including aquifer characterization. Chen and Zhang (2006) applied the EnKF to continuously update the hydraulic conductivity of both two- and three-dimensional synthetic models by assimilating dynamic pressure head observations. Camporese et al. (2011) applied the EnKF to infer the spatial distribution of hydraulic conductivity from electrical resistivity tomography monitoring of a three-dimensional synthetic tracer test experiment. Tong et al. (2013) used the EnKF in a synthetic two-dimensional aquifer to identify the hydraulic conductivity distribution by assimilating solute concentration measurements. Xu and Gómez-Hernández (2018) used the restart normal-score EnKF for the simultaneous identification of a contaminant source and the spatially-variable hydraulic conductivity in an aquifer. The method has been applied in synthetic aquifers by assimilating in time piezometric heads and concentrations from observation wells.

Many variants of the EnKF have been developed over time, such as the ensemble smoother (ES) proposed by van Leeuwen and Evensen (1996). Unlike the EnKF, which sequentially assimilates data over time, the ES incorporates all available information into a single global update step. Bailey and Baù (2012) used the ES to estimate spatially-variable hydraulic conductivity within a synthetic three-dimensional tilted v-shaped catchment system by assimilating water table elevation and streamflow data. Crestani et al. (2013) compared the capabilities of the EnKF and the ES to estimate the hydraulic conductivity assimilating observed concentrations. The two approaches have been tested in a two-dimensional synthetic aquifer where a tracer test is simulated. The authors conclude that EnKF always outperforms the ES due to iterative assimilations of information that helps to handle nonlinear and non-Gaussian conditions. With the aim to improve the ES performance for highly nonlinear applications, Emerick and Reynolds (2012; 2013) proposed the ensemble smoother with multiple data assimilation (ES-MDA), which iteratively assimilates the same data multiple times. The good performance of ES-MDA for inverse modelling have been confirmed in different studies (Todaro et al. 2019; 2021; 2022; D'Oria et al. 2021; Lam et al. 2020; Godoy, Napa-García, and Gómez-Hernández 2022). Xu et al. (2021) compared the ensemble smoother with multiple data assimilation (ES-MDA) and the restart EnKF for the simultaneous identification of a contaminant source and hydraulic conductivity using both piezometric heads and concentrations on a synthetic aquifer. The results showed that the ES-MDA performs better than the restart EnKF when using enough iterations, needing almost the same computational time.

While these studies has demonstrated the capability of ensemble-based methods to determine aquifer parameters, their application to real sites is still limited due to the complexity of field data collection. Chen et al. (2013) employed the parameter space EnKF and some variants of ES to characterize the hydraulic conductivity field of an aquifer by assimilating experimental tracer data obtained from the Integrated Field Research Challenge site in U.S. Department of Energy's Hanford 300 Area.

In this work, the ES-MDA is employed to infer the properties of a binary aquifer from concentration data obtained via an experimental tracer test. The data are collected in a laboratory sandbox that mimics a vertical cross-section of an unconfined aquifer. Glass beads of two different diameters reproduce a heterogeneous binary field, and fluorescein sodium salt is used as a tracer. The groundwater flow and transport processes are modeled with MODFLOW and MT3DMS, respectively. The software package genES-MDA (Todaro et al. 2022) was used to apply the ES-MDA procedure.

Different approaches are tested to estimate the aquifer parameters. First, the binary pattern of the true field is assumed unknown, and the ES-MDA is applied to directly estimate the hydraulic conductivity field. Another common approach to model subsurface characteristics is the conceptualization of the field using lithotypes or facies; constant properties are assigned to each lithotype. Kalman filter-based methods are optimal when working with Gaussian distributed parameters, and they are not suitable for estimating categorical variables, such as geological lithotypes. To handle the categorical parameter estimation through ES-MDA, it can be coupled with a truncated Gaussian method (Matheron et al. 1987). The main key of the truncated Gaussian model is the definition of the proportion of facies and their spatial distribution. The application of this approach for inverse modelling was firstly introduced by Wen et al. (2002) as an extension of the self-calibrating approach (Capilla et al. 1998, Wen et al. 1999, Franssen et al. 2002). Then, the truncated Gaussian methods have been linked to ensemble-based methods in history-matching problems (Liu and Oliver 2005; Agbalaka and Oliver 2008; Zhao, Reynolds, and Li 2008; Zhang et al. 2015), but they have only been applied to synthetic cases and considering the properties of the facies known.

In this work, the ES-MDA is coupled with a truncated Gaussian model (ES-MDA-T) to simultaneously estimate the pattern of the aquifer and the hydraulic and transport parameters of each facie. Both ES-MDA and ES-MDA-T are applied using a fully parametrized approach, parameters are estimated at each cell of the grid domain, and a pilot point approach, parameters are estimated at some points of the grid and then interpolated to obtain the solution over the whole field. To validate the methods proposed, a synthetic case that reproduces the sandbox experiment is developed and used to test different configuration of the inverse procedures. Then the experimental tracer test data are used to infer the characteristics of the sandbox field.

The paper is organized as follows: the next Section presents the ES-MDA procedure and its link with a truncated Gaussian model; Section 3 describes the sandbox and the laboratory and synthetic experiments; Section 4 summarizes all the tests performed using synthetic and experimental data; Section 5 outlines discussion and conclusion.

2. Methods

The methods applied in this work to solve the inverse problem are based on the ensemble smoother with multiple data assimilation (ES-MDA) technique, in some cases coupled with a Gaussian truncated model. The ES-MDA is a stochastic iterative approach that allows the estimation of a set of unknown parameters and their uncertainty from available observations of the state of the system. The description of the ES-MDA scheme is presented in detail by Emerick and Reynolds (2013), Evensen (2018) and Todaro et al. (2022); here, an overview of the method is given. Then the link between the truncated Gaussian model and the ES-MDA is presented.

2.1 ES-MDA

The ES-MDA is used to solve the inverse problem aimed at estimating the aquifer parameters assimilating observed tracer breakthrough curve data. The vector $\mathbf{X} \in \Re^{N_P}$ contains the aquifer parameters to be estimated, while the vector of observations $\mathbf{D} \in \Re^{m}$ contains the tracer concentrations measured at sparse sampling locations in the aquifer at different times. The method requires the relationship between parameters and observations to be known; this is given by a forward model that simulates the flow (MODFLOW) and transport processes (MT3DMS). The procedure consists of an initialization phase and then proceeds with an iterative loop made up of two steps.

Initialization phase

The first ingredient of the ES-MDA is the definition of an initial ensemble of parameters. The size of the ensemble, N_e, should be large enough to be statistical representative of the problem at hand and as small as possible with the aim to limit the computational burden. The characteristics of the initial ensemble of parameters allow to take into account prior information, when available.

Another preliminary step is to specify an ensemble of measurement errors $\boldsymbol{\varepsilon} \in \Re^{m \times N_e}$, they are usually assumed to be uncorrelated and drawn from a Gaussian distribution with zero mean and given standard deviation. The ES-MDA also requires defining a priori the number of iterations to be performed, N, and a vector of coefficients $\boldsymbol{\alpha} = (\alpha_1, \alpha_2, \dots, \alpha_N)$ that apply to the measurement errors and control the parameter change from one step to another. A gradual decrease of $\boldsymbol{\alpha}$ during the iterative process improves the performance of the method as it gradually reduces the measurement errors helping to avoid overfitting in the first updates. Several schemes can be used to define the set of $\boldsymbol{\alpha}$, but they must satisfy the condition:

$$\sum_{i=1}^{N} \frac{1}{\alpha_i} = 1$$

After the initialization step, the procedure follows with two iterative steps.

Forecast step

At each iteration i, the state of the system coinciding with the available observations, $\mathbf{Y}_{j,i}$, are obtained for each realization j of the ensemble of parameters, $\mathbf{X}_{j,i}$, by means of the forward model:

$$\mathbf{Y}_{j,i} = g(\mathbf{X}_{j,i}),$$

where the operator $g(\cdot)$ includes the forward model run and the functions used to extract the predictions at the same spacetime locations where observations were collected.

Update step

During the update step, the ensemble of parameters is updated following the equation:

$$\mathbf{X}_{i+1} = \mathbf{X}_i + \frac{\mathbf{C}_{\mathbf{XY}}^{i}}{\mathbf{C}_{\mathbf{YY}}^{i} + \alpha_i \mathbf{R}} \times \left(\mathbf{D} + \sqrt{\alpha_i}\boldsymbol{\varepsilon} - \mathbf{Y}_i\right),$$

where $\mathbf{C}_{\mathbf{XY}}^{i} \in \Re^{N_P \times m}$, $\mathbf{C}_{\mathbf{YY}}^{i} \in \Re^{m \times m}$ and $\mathbf{R} \in \Re^{m \times m}$ are the cross-covariance between parameters and predictions, the auto-covariance of the predictions and the auto-covariance of the measurement errors, respectively. $\mathbf{R}$ is a diagonal matrix containing the error variances, $\mathbf{C}_{\mathbf{XY}}^{i}$ and $\mathbf{C}_{\mathbf{YY}}^{i}$ are computed from the parameters and predictions ensembles as:

$$\mathbf{C}_{\mathbf{XY}}^{i} = \frac{1}{N_e - 1}\sum_{j=1}^{N_e}\left(\mathbf{X}_{j,i} - \overline{\mathbf{X}}_i\right)\left(\mathbf{Y}_{j,i} - \overline{\mathbf{Y}}_i\right)^T$$

$$\mathbf{C}_{\mathbf{YY}}^{i} = \frac{1}{N_e - 1}\sum_{j=1}^{N_e}\left(\mathbf{Y}_{j,i} - \overline{\mathbf{Y}}_i\right)\left(\mathbf{Y}_{j,i} - \overline{\mathbf{Y}}_i\right)^T,$$

where $\overline{\mathbf{X}}_i$ and $\overline{\mathbf{Y}}_i$ are the ensemble means of parameters and predictions, respectively.

The procedure repeats until the last iteration after making $\mathbf{X}_i = \mathbf{X}_{i-1}$.

To avoid the appearance of negative values during the update phase, which can be inconsistent for some types of parameters, a space transformation can be applied. In this study, the ensemble of parameters is transformed in the logarithmic space before the update and back-transformed into its physical space after the update.

The total number of runs of the forward model, n_t, required by ES-MDA depends on the ensemble size and the number of iterations: $n_t = N \cdot N_e$. Therefore, it is crucial to use a small ensemble and at the same time avoiding undersampling problems that leads to divergence and the appearance of long spurious correlations. Covariance localization approaches can be applied to mitigate the appearance of long-range spurious correlations and increases the rank of the covariance matrices, which are rank deficient when the number of parameters is higher than the ensemble size.

Covariance localization is applied by element-wise multiplication of the original covariance matrices with correlation matrices reducing the correlations between points for increasing distances (Hamill, Whitaker, and Snyder 2001; Anderson 2007; Y. Chen and Oliver 2010).

Furthermore, to avoid overshooting, a linear relaxation can be applied on the ensemble of parameters at the end of each update step:

$$\widehat{\mathbf{X}}_{\mathrm{i+1}} = (1-\mathrm{w})\mathbf{X}_{\mathrm{i+1}} + \mathrm{w}\mathbf{X}_{\mathrm{i}},$$

where w is a relaxation coefficient between 0 and 1.

2.2 The ES-MDA-T: linking the ES-MDA and a truncated Gaussian model

In this paper, the ES-MDA is coupled with the truncated Gaussian model with the aim of characterizing a binary field. The spatial distribution of the two facies and their main properties are simultaneously estimated. The proportion of the two lithotypes is assumed known. The truncated Gaussian model consists of thresholding a Gaussian random function using a threshold defined to match the proportions of the facies.

In this case, the vector of unknown parameters is $\mathbf{X} = (\mathbf{P}_1, \mathbf{P}_2,\ \mathbf{F})$, where $\mathbf{P}_1$ and $\mathbf{P}_2$ are the properties of the two facies to be estimated (e.g. hydraulic conductivities, longitudinal dispersivities of the two facies, etc.), while $\mathbf{F} = (\mathrm{F}_1, \mathrm{F}_2, \ldots, \mathrm{F}_{N_C})$ is the vector containing the categorical variables for each cell of the discretized domain. Therefore, the number of unknown parameters $\mathrm{N_P}$ is equal to the number of aquifer parameters to be estimated (for the two facies) plus the total number of cells of the model grid (N_C) corresponding to the categorical variables. The categorical variable can take the values 1 or 2. The cells with categorical value 1 assume the properties $\mathbf{P}_1$, while the cells with categorical value is 2 assume properties $\mathbf{P}_2$. The vector of observations $\mathbf{D}$ is the same as in the previous section.

This procedure allows for estimating categorical variables using the ES-MDA. The modification to the ES-MDA loop to incorporate the truncated Gaussian model into the process is described below.

<u>Initialization phase</u>

The initial ensemble of parameters is generated using random values drawn from a Gaussian distribution for the realizations of the aquifer parameters ($\mathbf{P}_1$ and $\mathbf{P}_2$) and random Gaussian fields for the definition of the spatial distribution of the facies; let's call this initial ensemble of Gaussian random fields $\tilde{\mathbf{F}} = (\tilde{\mathrm{F}}_1, \tilde{\mathrm{F}}_2, \ldots, \tilde{\mathrm{F}}_{N_C})$. The proportion between facies must be defined a priori on the basis of available information and expert knowledge. The ensemble of measurement errors and the vector of coefficients $\boldsymbol{\alpha}$ are defined as described in the previous section.

The following iterative loop is the same as the standard ES-MDA method, but an additional step named "truncation step" is introduced before the forecast step.

<u>Truncation step</u>

The truncation step consists in thresholding the Gaussian field to obtain a binary field; this step allows to transform the continuous variables estimated by ES-MDA into categorical variables. At each iteration i and for each realization of parameters j, the categorical field $\mathbf{F}_{i,j}$ is obtained by truncating the Gaussian field $\tilde{\mathbf{F}}_{i,j}$ using as threshold the percentile corresponding to the facies proportion. Then, the continuous Gaussian field is transformed into a categorical one by replacing each value of $\tilde{\mathbf{F}}_{i,j}$ with 1, if it is below or equal to the threshold, and 2 otherwise. In Figure 1, an example of a Gaussian field and the associated binary field after truncation is shown.

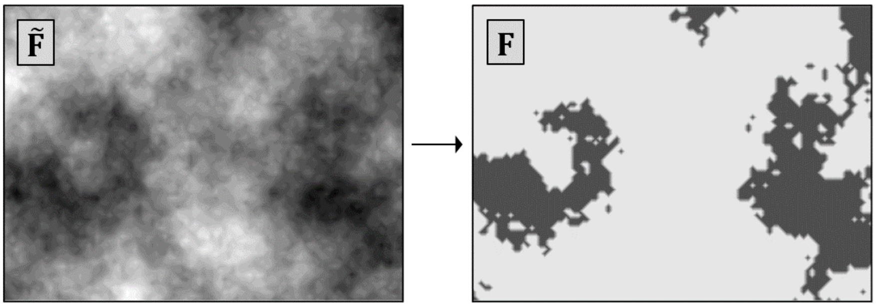

Figure 1 - Truncated Gaussian model performed considering a facies proportion equal to 76%. The Gaussian field is on the left and the truncated field is on the right.

Forecast step

At each iteration i, the predictions $\mathbf{Y}_{j,i}$ are obtained for each realization j of the ensemble of parameters, $\mathbf{X}_{j,i} = (\mathbf{P}_1, \mathbf{P}_2, \mathbf{F})$,

$$\mathbf{Y}_{j,i} = g(\mathbf{X}_{j,i}).$$

At each cell of the grid, $\mathbf{P}_1$ parameters are assigned if the categorical value of the cell is 1, and $\mathbf{P}_2$ are assigned if the categorical value of the cell is 2.

Update step

During the update step, the ensemble of parameters, $\tilde{\mathbf{X}}_{j,i} = (\mathbf{P}_1, \mathbf{P}_2, \ \tilde{\mathbf{F}})$ is updated in the continuous space:

$$\tilde{\mathbf{X}}_{i+1} = \tilde{\mathbf{X}}_i + \frac{\mathbf{C}_{\mathbf{XY}}^{i}}{\mathbf{C}_{\mathbf{YY}}^{i} + \alpha_i \mathbf{R}} \times \left(\mathbf{D} + \sqrt{\alpha_i}\boldsymbol{\varepsilon} - \mathbf{Y}_i\right).$$

The key difference with the standard implementation is that the updates are applied to the underlying continuous Gaussian fields and not to the conductivity fields, which, in this case, are binary. Then the procedure repeats from the truncation step until the end of the iterative process.

3. Description of the experiment

3.1 Sandbox experiment

The tracer test used to collect the observations to solve the inverse problem is reproduced in a laboratory sandbox set up in the hydraulic laboratory of the University of Parma, Italy (Figure 2). The experimental device mimics a vertical cross-section of an unconfined heterogeneous aquifer and the device has been used to develop several laboratory tests (Cupola, Tanda, and Zanini 2015; Citarella et al. 2015; Todaro et al. 2021; Z. Chen et al. 2018; 2021; 2022). The sandbox has a width of 120 cm, a height of 73 cm, and a thickness of 14 cm; it is made of polymethyl methacrylate (PMMA) plates with a thickness of 2 cm for the lateral sides and 3 cm for the bottom lid. The sandbox is divided in three parts along the longitudinal direction: an upstream tank, a central chamber that contains the porous medium and a downstream tank. The flow into the experimental device is governed by the water levels at the upstream and downstream tanks, which are equal to 62.5 cm and 61 cm above the horizontal bottom of the tank, respectively. The porous media consists of glass beads with two different diameters of about 1 mm and 4 mm, which reproduce a binary field. Fluorescein sodium salt is employed as conservative tracer. The PMMA walls of the device allow to collect concentration data by interpreting pictures taken during the experiment. The picture RGB values are converted to concentrations through an image processing technique (Citarella et al. 2015).

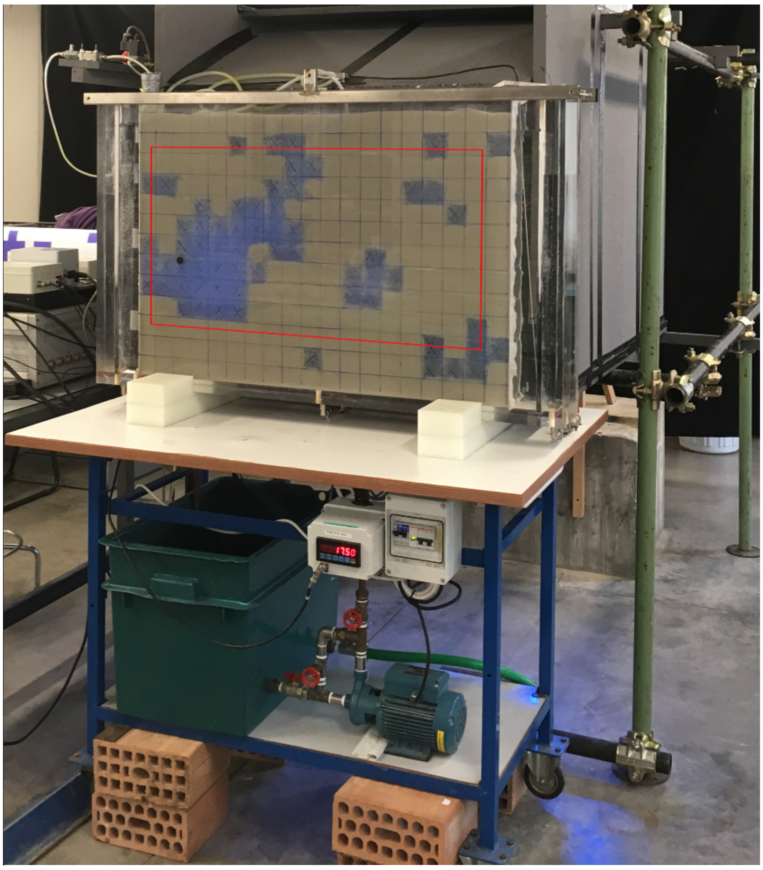

Figure 2 – Picture of the front side of the experimental sandbox. The red rectangle outlines the area where experimental data are collected.

At the beginning of the experiment (initial condition) the porous medium within the sandbox had a homogeneous concentration of fluorescein sodium salt of 25 mg/l. The tracer test performed had a duration of 4000 s; during this time the fluorescein concentration progressively decreases within the sandbox as clean water enters the system. The experiment ended when tracer concentration was zero everywhere. Pictures are collected with a time step of 5 seconds and converted in concentration data at each pixel of the images. Breakthrough curves recorded at 64 monitoring points with a discretization time of 75 seconds are used as observations in the inverse procedure. As example, Figure 3 shows the concentration fields obtained from the analysis of the images in four instants from the beginning of the test.

During the experiment, the flow stopped accidentally for about 855 s after 985 s since the start of the test. This was likely caused by a clogged drain in the downstream tank leading to a rise in the downstream water level and resulting in no gradient in the sandbox during the clogging period. The model that simulates the experiment also takes into account the period of no-flow considering a transient boundary condition downstream. Groundwater flow and mass transport were modeled with MODFLOW 2005 (Harbaugh, 2005) and with MT3DMS (Zheng and Wang, 1999), respectively. The domain is discretized into a uniform grid of 1 cm resolution (70 layers, 97 columns and 1 row).

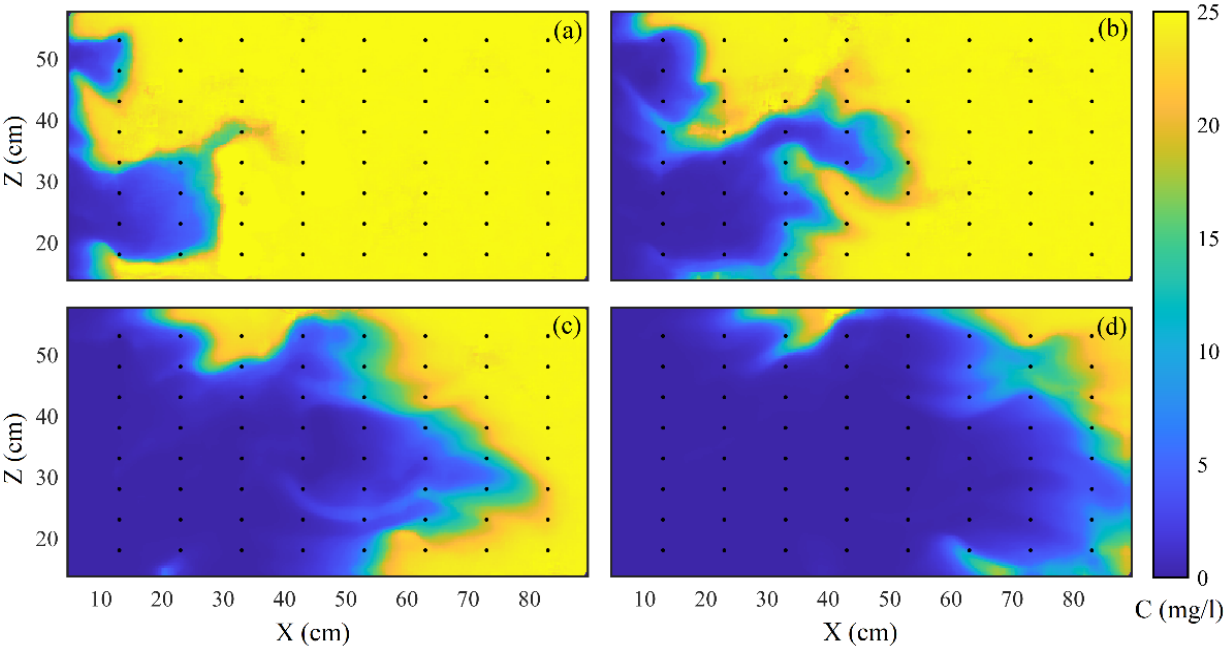

Figure 3 - Concentration field from the image process collected 250 (a), 500 (b), 1500 (c) and 2250 s (d) after the start of test. Flow direction is from left to right. The black dots indicate the monitoring points where observations are collected to perform the inverse procedure.

3.2 Synthetic experiment

Before applying the different methods to the sandbox experiment, a synthetic case was performed with the aim of evaluating the capability of the proposed approaches to infer the aquifer characteristics and find the optimal configuration of the inverse algorithm. The synthetic case mimics the sandbox experiment; the reference hydraulic conductivity field is depicted in Figure 4. It is a binary field characterized by two different facies, named Facies 1 and Facies 2. The same numerical model developed to simulate the experimental test is used as forward model; the reference solution is obtained using the parameters reported in Table 1. The observed concentrations used for the inverse modeling are collected at the same spacetime locations considered for the experimental data: 64 breakthrough curves discretized in 54 time steps.

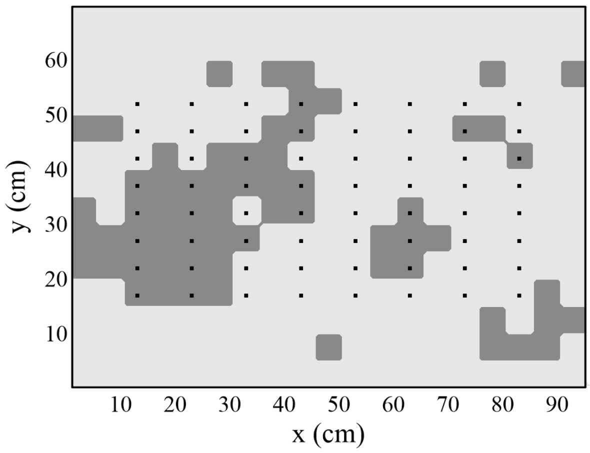

Figure 4 - Reference conductivity field of the synthetic case. Light gray represents Facies 1, dark gray represents Facies 2. Black squares indicate the monitoring points.

Table 1 - Transport and hydraulic parameters of the numerical model used to set up the synthetic case study. HK is the horizontal hydraulic conductivity, n is the porosity, Ss is the specific storage coefficient, α_L is the longitudinal dispersivity and α_T is the transverse dispersivity.

	Facies 1	**Facies 2**
HK (cm/s)	0.65	10
N (-)	0.37	0.37
HK/VK (-)	10	10
Ss (cm^{-1})	10^{-4}	10^{-4}
α_L (cm)	0.1	0.2
α_T/α_L (-)	0.05	0.05

4. Applications

Several tests were performed to compare the different approaches and the different settings of the ES-MDA algorithm. The analyses were initially performed using the dataset of the synthetic experiment and then the laboratory data. For all tests, the observations used in the inverse modeling are the breakthrough curves collected at the 64 monitoring points depicted in Figure 4 and discretized in 54 time steps (number of observations m is 3456). The first analyses employ the ES-MDA to estimate directly the hydraulic conductivity field (HK_1, HK_2, …,$\mathrm{HK}_{\mathrm{N_P}}$); then, the ES-MDA-T is used incorporating the extra information that the medium is binary and, therefore, it focuses in identifying the spatial distribution of the two facies (F_1, F_2, …,$\mathrm{F}_{\mathrm{N_C}}$) and 5 aquifer parameters: the hydraulic conductivity (HK_{F1} and HK_{F2}) and longitudinal transport dispersivity ($\alpha_{L,F1}$

and $\alpha_{L,F2}$) of the two facies and the ratio between the transversal and longitudinal dispersivity equal for the two facies (α_T/α_L). The proportion between the two facies is assumed known for all tests and equal to 76% for Facies 1 and 24% for Facies 2.

Both the ES-MDA and the ES-MDA-T are applied using a fully parameterized approach and a pilot-point method aimed at reducing the number of unknown parameters. For the fully parameterized approach, the parameters are estimated at each cell of the model grid (N_P=6790 for the ES-MDA, N_P=6795 for the ES-MDA-T); for the pilot-point method, the parameters are estimated at 266 points uniformly distributed over the field (N_P=266 for ES-MDA, N_P=271 for ES-MDA-T). The full map of parameters is obtained by assigning to each cell of the model grid the value of the closest pilot point. (This type of interpolation will result in a blocky distribution of the conductivities that would resemble the way the sandbox was filled in with the binary media). The ensemble size considered (number of realizations of parameters) is 1000 for the fully parametrized approach and 100 for the pilot-point one.

For all tests, the measurement error ε is normally distributed with zero mean and variance $5 \cdot 10^{-2}$ mg/l. The ES-MDA and ES-MDA-T are run with 6 iterations and decreasing α=[364; 121.3; 40.4; 13.5; 4.5; 1.5]. Covariance localization is applied considering tapering functions that gradually reduce the correlations based on the spatial distance between parameters and predictions, and predictions and predictions and modify the covariance matrices applying a scale factors from 1 (no-correction) to 0 (zero correlation) for distances from 0 cm to 120 cm. The linear relaxation is applied with the coefficient w = 0.2 for the synthetic data and with w = 0.25 for the experimental data.

The specific configuration of each test and the results are presented in the following.

4.1 Synthetic case study

4.1.1 Test 1.1: ES-MDA for the estimation of the hydraulic conductivity field following a fully parameterized approach

The ES-MDA is applied for the estimation of the hydraulic conductivity field in each cell of the model domain considering the remaining hydraulic and transport parameters known. Two tests were performed starting from different types of initial ensemble of parameters, all other variables being equal. The size of the ensemble is 1000 for both tests. The first test (Test 1.1A) uses homogeneous fields as initial ensemble of parameters; the hydraulic conductivity of each realization is constant and selected randomly from a uniform distribution, HK ∈ U[0.1,9]. For the second test (Test 1.1B), the initial ensemble of parameters is made up of Gaussian fields generated using isotropic exponential variograms with random parameters: the mean μ, variance σ and range of correlation h are drawn from the following uniform distributions: μ ∈ U[0.5,0.7], σ ∈ U[60,365], h ∈ U[0.05,2]. Figure 5 shows some realizations of the initial ensembles of parameters and the results of the inverse procedure for both tests. The results refer to the mean field obtained from the ensemble at the last iteration of the ES-MDA procedure. The map of coefficient of variations is also reported. The RMSE between observed and predicted concentrations is 2.7 mg/l and 2.1 mg/l for Test 1.1A and Test 1.1B, respectively.

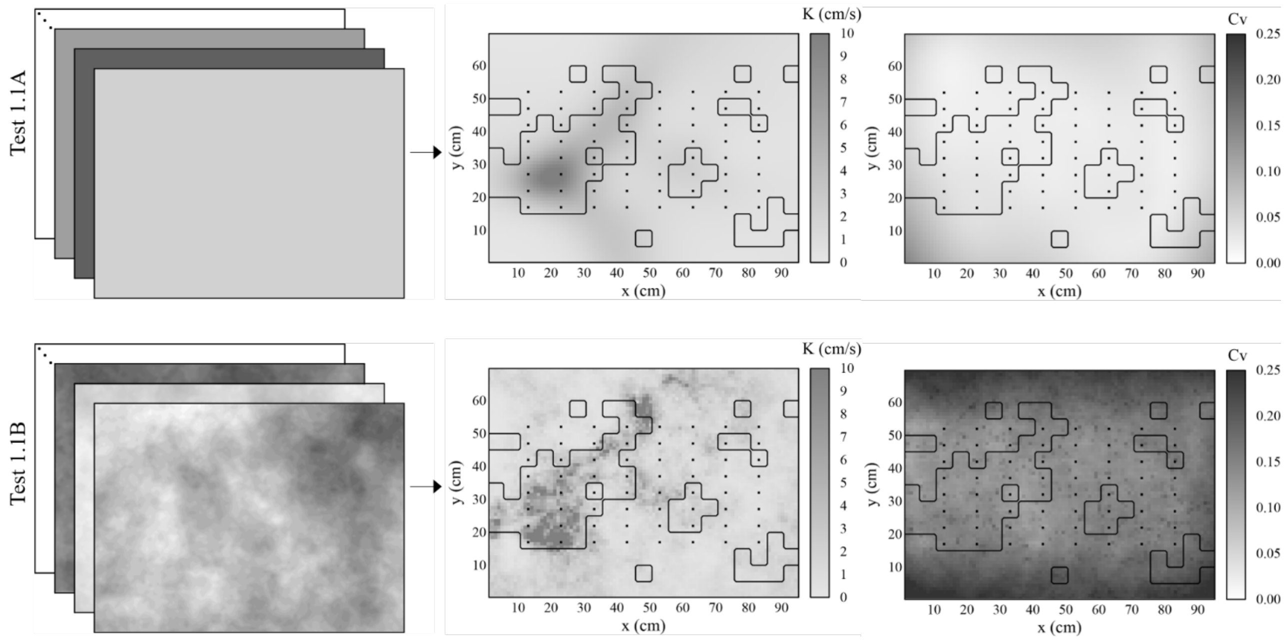

Figure 5 - Test 1.1: Examples of realizations of the initial ensemble of parameters for Test 1.1A and Test 1.1B (left); estimated fields in terms of ensemble mean (middle) and map of the coefficient of variation (right). The black squares indicate monitoring points. The solid line reproduces the outline of the two facies of the actual field.

4.1.2 Test 1.2: ES-MDA for the estimation of the hydraulic conductivity using a pilot point approach

The ES-MDA is applied for the estimation of the hydraulic conductivity field at 266 pilot points (Figure 6). The ensemble size is 100; the initial realizations of parameters are a subset of the ensemble used in Test 1.1B, from which the values at the pilot point locations were selected.

Figure 6 shows the mean field obtained from the ensemble at the last iteration and the map of the coefficient of variation computed from the ensemble. The RMSE between observed and predicted concentrations is 2.1 mg/l.

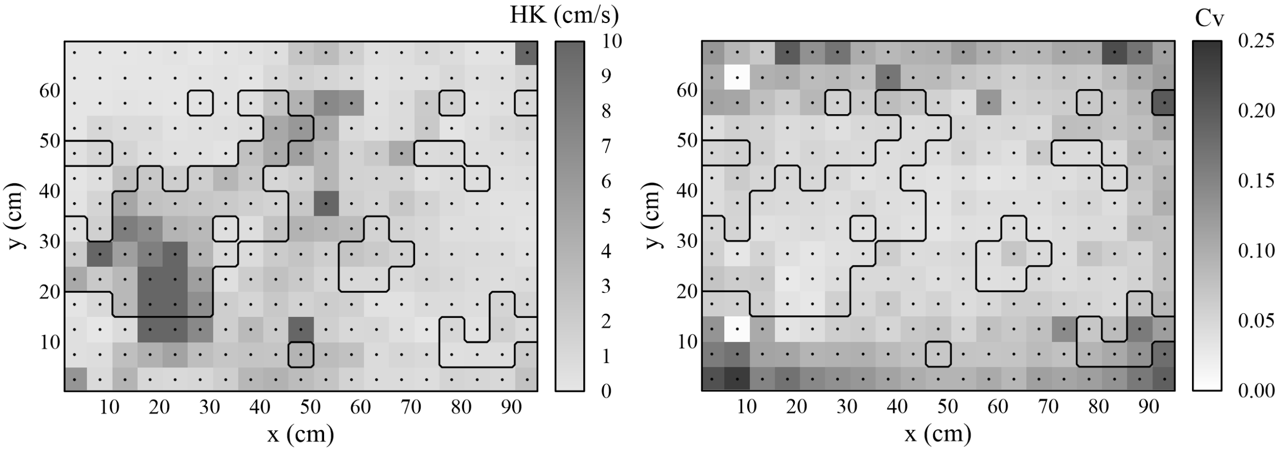

Figure 6 - Test 1.2: Estimated binary field by means of the ES-MDA using a pilot point approach; the ensemble mean (left) and the coefficient of variation (right) are reported. The black dots indicate the pilot points.

4.1.3 Test 1.3 ES-MDA-T for the characterization of the binary field following a fully parameterized approach

The ES-MDA is linked with the truncated Gaussian model to simultaneously estimate the spatial distribution of the two-facies and their main properties. In Test 1.3 the fully parameterized approach is adopted. The ensemble size is 1000 and the initial realizations of the hydraulic and transport parameters of the two facies are drawn from Gaussian distributions with different mean and variance defined as follows: $HK_{F1} \in \mathcal{N}[0.7,0.01]$; $HK_{F2} \in \mathcal{N}[7,1]$; $\alpha_{L,F1} \in \mathcal{N}[0.1,4\cdot10^{-3}]$; $\alpha_{L,F2} \in \mathcal{N}[0.2,4\cdot10^{-3}]$; $\alpha_T/\alpha_L \in \mathcal{N}[0.05, 1\cdot10^{-3}]$. The initial realizations of the field $\tilde{\mathbf{F}}$ are Gaussian random fields with zero mean and standard deviation of 1 generated using isotropic Gaussian variograms with correlation range randomly selected from a uniform distribution $h \in U[10,60]$.

Figure 7 shows the solution in terms of best estimate represented in each cell by the mode of the ensemble of parameters. The accuracy is given by the percentage of realizations that agree with the best estimate. For most cells, almost all realizations estimate the true categorical variable; the lowest accuracy is found at the interface between the two materials.

Table 2 summarizes the actual and estimated hydraulic and transport parameters with their uncertainty; the approach shows very good performance in reproducing all the properties of the two facies. The RMSE between observed and predicted concentrations is equal to 1.53 mg/l.

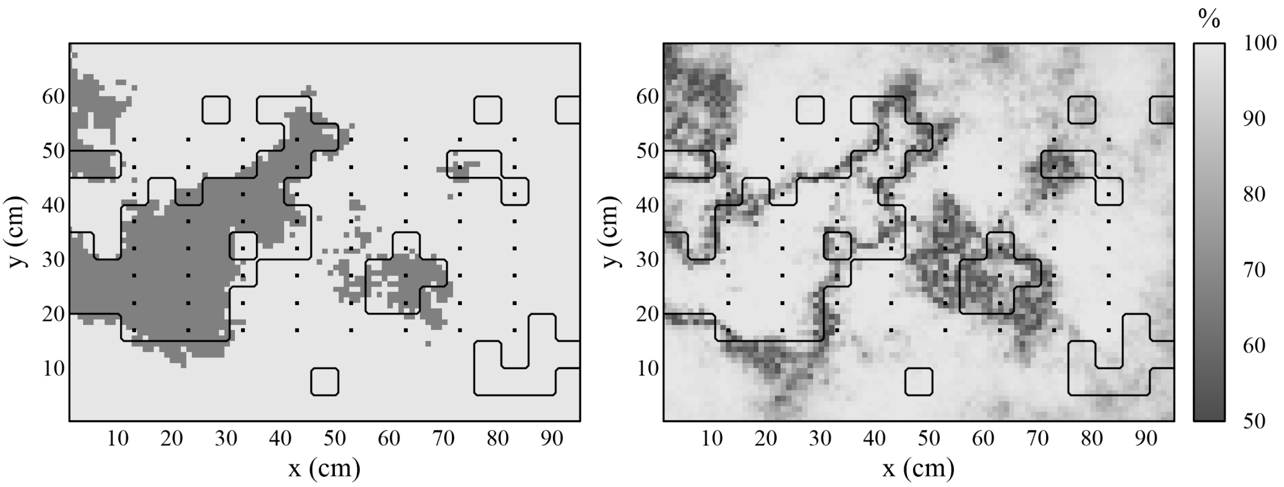

Figure 7 – Test 1.3: Best estimate of the binary field using the ES-MDA-T (left); light gray represents Facies 1, dark gray represents Facies 2. Accuracy of the estimate as proportion of realizations correctly identifying the reference facies (right). Black squares indicate monitoring points. The solid line reproduces the outline of the two facies of the actual field.

Table 2 – Test 1.3: Actual and estimated parameters of the two facies. The ensemble mean and the 95% uncertainty interval are reported.

	Actual	**Estimated**
HK_{F1} (cm/s)	0.65	0.69 ± 0.04
HK_{F2} (cm/s)	10	9.92 ± 0.88
$\alpha_{L,F1}$ (cm)	0.1	0.097 ± 0.022
$\alpha_{L,F2}$ (cm)	0.2	0.199 ± 0.022
α_T/α_L	0.05	0.047 ± 0.011

4.1.4 Test 1.4 ES-MDA-T for the characterization of the binary field using the pilot point approach

Test 1.3 is repeated using the pilot point method. The initial ensemble of parameters is made up of 100 realizations that are a subset of the initial ensemble of Test 1.3: the values at the pilot point locations are extracted from the fully parametrized field. In Figure 8 the resulting binary field (best estimate) is depicted with its accuracy (percentage of realizations that agree with the reference). Most of the true categorical parameters are well reproduced and the estimation accuracy is 100% in almost the whole field. The hydraulic and transport parameters of the two facies are reported in Table 3. The RMSE between observations and prediction is equal to 2.2 mg/l.

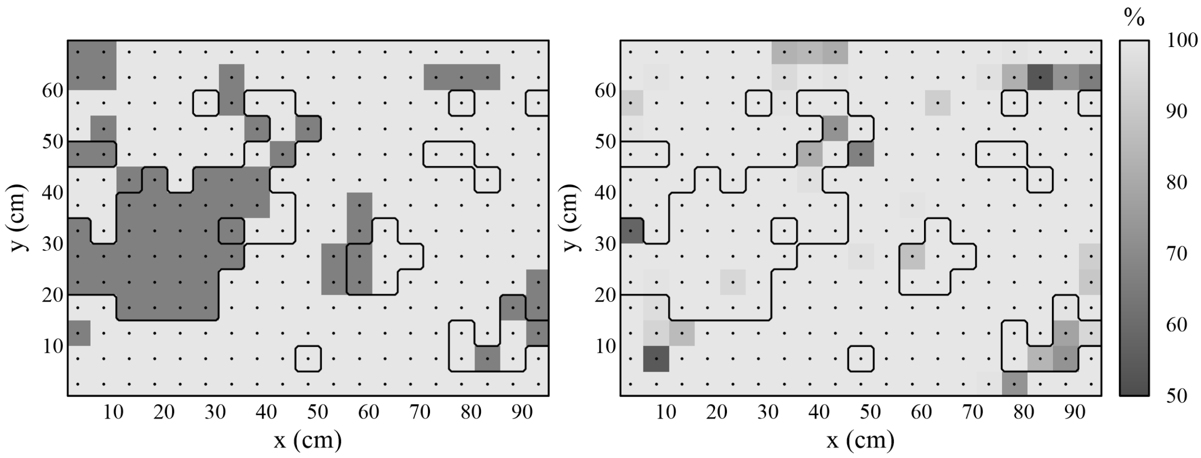

Figure 8 - Test 1.4: Best estimate of the binary field by means of the ES-MDA-T using a pilot point approach (left); light gray represents Facies 1, dark gray represents Facies 2. Accuracy of the estimate (right). Black dots indicate the pilot points. The solid line reproduces the outline of the two facies of the actual field.

Table 3 – Test 1.4: Actual and estimated parameters of the two facies. The ensemble mean and the 95% uncertainty interval are reported.

	Actual	**Estimated**
HK_{F1} (cm/s)	0.65	0.740 ± 0.005
HK_{F2} (cm/s)	10.00	10.50 ± 0.10
$\alpha_{L,F1}$ (cm)	0.10	0.080 ± 0.001
$\alpha_{L,F2}$ (cm)	0.20	0.210± 0.002
α_T/α_L	0.050	0.076 ± 0.001

4.2 Experimental case study

The results obtained from the synthetic case analyses pointed out that the best performance is achieved using the ES-MDA-T approach. Therefore, tests performed using data from the sandbox experiment only consider the approach that link ES-MDA with the truncated Gaussian model.

4.2.1 Test 2.1: ES-MDA-T for the characterization of the binary field following a fully parameterized approach

The ES-MDA-T is applied for the simultaneous estimation of the spatial distribution of the two facies and their properties using the experimental data. The same settings and ensembles of the synthetic Test 1.3 are used. Figure 9 shows the results obtained by truncation of the ensemble mean of the field, where 73% of the estimated parameters match the experimental distribution of the facies. The estimated hydraulic and transport parameters with their uncertainty are reported in Table 4. The RMSE between observed and predicted concentrations is equal to 3.2 mg/l.

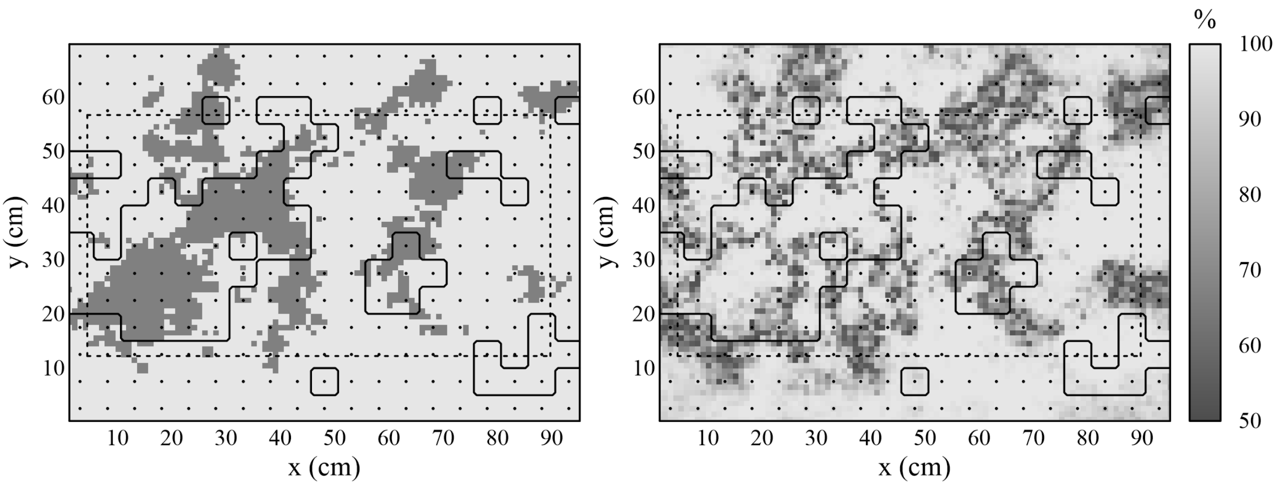

Figure 9 - Test 2.1: Best estimate of the binary field (right) obtained by means of the ES-MDA-T using experimental data; light gray represents Facies 1, dark gray represents Facies 2. . Accuracy of the estimate (right). The black squares indicate monitoring points; the dashed line denotes the portion of the field where experimental data are available. The solid line reproduces the outline of the two facies of the actual field.

Table 4 - Test 2.1: Estimated parameters of the two facies. The ensemble mean and the 95% uncertainty interval are reported.

	Facie1	**Facie2**
HK (cm/s)	0.68 ± 0.03	12.53 ± 0.72
α_L (cm)	0.15 ± 0.03	0.20 ± 0.02
α_T/α_L	0.21 ± 0.05	

4.2.2 Test 2.2: ES-MDA-T for the characterization of the binary field using a pilot point approach

In the second experimental case study, the same configuration of Test 1.4 is employed. The inverse problem is solved by means of the pilot point method. The results are depicted in Figure 10; only a portion of the field is well reproduced. In particular, the ES-MDA-T fails to correctly estimate the actual categorical variable for the upper part of the field where no observation data are available.

Table 5 reports the estimated hydraulic and transport parameters with their uncertainty. The RMSE between observed and predicted concentrations is equal to 2.9 mg/l.

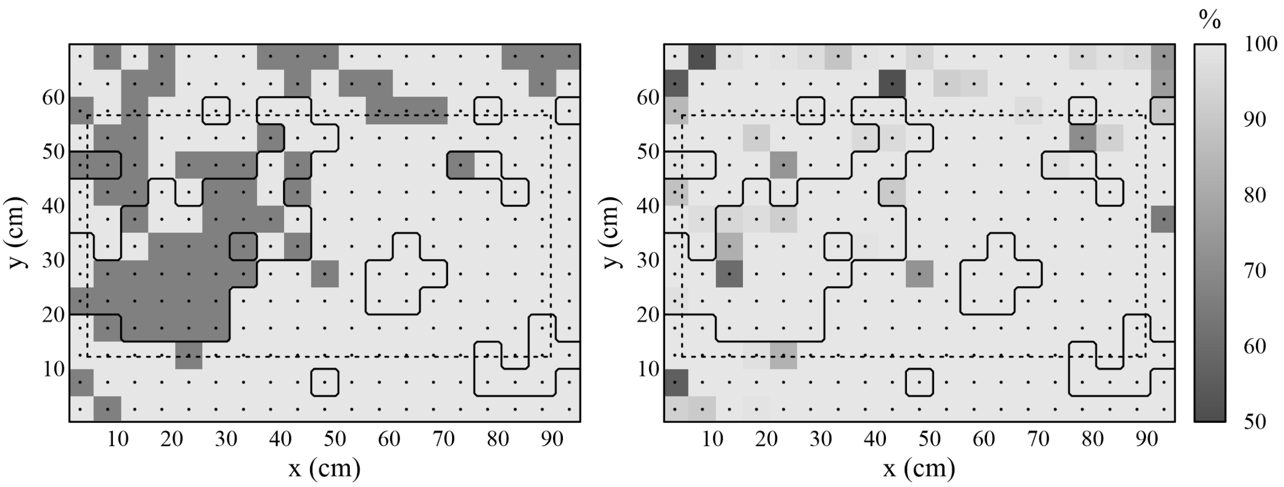

Figure 10 - Test 2.2: Best estimated of the experimental binary field by means of the ES-MDA-T using a pilot point approach (left); light gray represents Facies 1, dark gray represents Facies 2. Accuracy of the estimate (right). Black dots indicate the pilot points; the dashed line denotes the portion of the field where experimental data are available.

Table 5 - Test 2.2: Estimated parameters of the two facies. The ensemble mean and the 95% uncertainty interval are reported.

	Facie1	**Facie2**
HK (cm/s)	0.770 ± 0.003	11.10 ± 0.05
α_L (cm)	0.120 ± 0.001	0.200 ± 0.001
α_T/α_L	0.310 ± 0.001	

4.2.3 Test 2.3: ES-MDA-T for the characterization of a three-facies field following a parameterized approach

The third test is performed considering that the experimental field is made of three materials. This follows the assumption that there is a mixing zone at the interface between the two facies made up of 1 mm or 4 mm diameter glass beads. The mixing zone, named Facies 3, has different characteristics from Facies 1 and Facies 2. The ES-MD-T is applied to estimate the spatial distribution of the three facies and their properties. The vector of unknown parameters is $\mathbf{X} = (\mathbf{P}_1, \mathbf{P}_2, \mathbf{P}_3\ \ \mathbf{F})$, where $\mathbf{P}_1$, $\mathbf{P}_2$ and $\mathbf{P}_3$ are the vectors containing the parameters of the three facies, $\mathbf{F}$ is the vector of categorical variables for each cell of the discretized domain. The categorical variable can take the values 1, 2 or 3. The cells with categorical value 1 assume the properties $\mathbf{P}_1$, the cells with categorical value 2 assume the properties $\mathbf{P}_2$ and when the value is 3, the parameters $\mathbf{P}_3$ are used. The vector of observations $\mathbf{D}$ is the same as the previous experimental tests. The truncation of the Gaussian field is performed defining two thresholds that match the proportions between the three facies. It is assumed that the 75% of the field is occupied by Facies 1, 17% by Facies 2 and 8% by Facies 3. The two thresholds are equal to the 75th-percentile (Thr_1) and 83th-percentile (Thr_2) of the values of the Gaussian field to be truncated. The continuous variables of the Gaussian function are transformed into categorical variables replacing each value with 1 if it is below Thr_1, 2 if it is above

Thr$_2$ and 3 otherwise. The same settings and initial ensemble of Test 2.1 are employed, but two additional parameters are estimated: the hydraulic conductivity (HK_{F3}) and longitudinal dispersivity ($\alpha_{L,F3}$) of Facies 3. The initial ensemble of the properties of Facies 3 are drawn from Gaussian distributions with different mean and variance defined as follows: $HK_{F3} \in \mathcal{N}[5, 0.5]$ and $\alpha_{L,F3} \in \mathcal{N}[0.4,0.05]$.

Figure 11 and Table 6 report the results of the inverse procedure. The RMSE between observed and predicted concentrations is 3.2 mg/l.

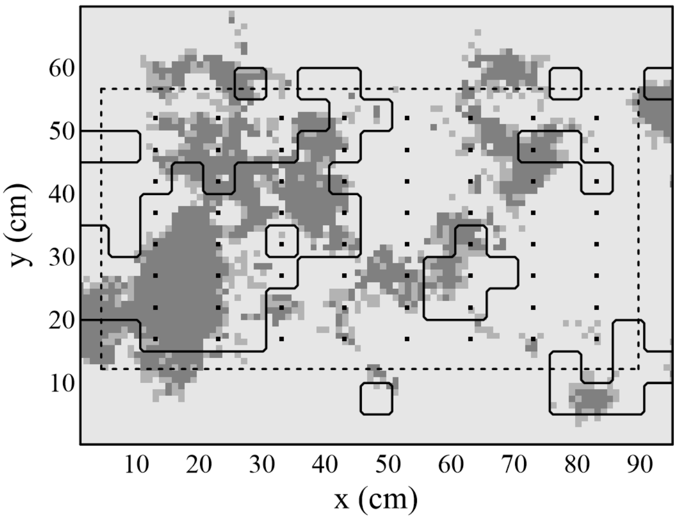

Figure 11 - Test 2.3: Estimated three-facies field by means of the ES-MDA-T using experimental data; the three shades of gray represent Facie1, Facie3 and Facie2, respectively. The black squares indicate monitoring points; the dashed line denotes the portion of the field in which experimental data are available. The solid line reproduces the outline of the two facies of the actual field.

Table 6 – Test 1.3: Estimated parameters of the three facies. The ensemble mean and the 95% uncertainty interval are reported.

	Facie1	**Facie2**	**Facie3**
HK (cm/s)	0.72 ± 0.03	12.26 ± 0.72	6.44 ± 0.57
α_L (cm)	0.07 ± 0.02	0.16 ± 0.02	0.25 ± 0.03
α_T/α_L	0.18 ± 0.04		

5. Discussion and Conclusions

The ensemble smoother with multiple data assimilation was applied to characterize a binary aquifer by means of experimental tracer test data. First, the ES-MDA was used to infer the hydraulic conductivity field unaware that it was binary and assuming the rest of hydraulic and transport parameters known. Then, the ES-MDA was linked with a truncated Gaussian model for the simultaneous estimation of categorical variables, which reproduce the two-facies field, and the properties of each facies. A fully parameterized approach and a pilot point approach were considered in the analysis. Initially, a synthetic case study that mimics the laboratory experiment was developed to test the capability of the proposed procedures. It is noteworthy that the observation errors assumed for the synthetic case are large and comparable with the experimental ones used for the laboratory case study. Test 1.1 aimed at the estimation of the hydraulic conductivity field using a fully-parameterized approach by assimilating observed breakthrough curves. The effect of the characteristics of the initial ensemble of parameters was investigated: Test 1.1A was performed considering an initial ensemble consisting of random homogeneous fields, while Test 1.1B considers Gaussian fields generated using exponential variograms with random parameters. The results show that Test 1.1B performs better in terms of RMSE between observed and predicted concentrations. Test 1.1A estimate a smoother field than Test 1.1B; the portions of the field with low and high permeability are fairly identified, but not the actual distribution of the two facies. On the contrary, Test 1.1B better reproduces the complexity of the actual field and the discontinuities between the two facies. In both tests, the coefficient of variation is higher at the top and bottom of the field, due to the absence of observation points in these portions of the aquifer. Therefore, the initialization of the procedure, in terms of the initial ensemble of parameters, affects the solution. This is stressed by the ensemble size; the smaller it is, the more the solution may depend on the initial configuration. The size of the ensemble should be related to the number of parameters to be estimated; in this case, the number of realizations is equal to 1000, and the number of parameters to be estimated is 6795. This may lead to rank-deficient covariance matrices, since they are computed from the ensembles, and therefore covariance localization techniques must be used to mitigate this effect. Hence, the use of a well-defined initial ensemble of parameters and covariance localization techniques allows reducing the number of realizations. This leads to a remarkable reduction of the computational burden. For instance, a gradient-based optimization method needs to run the forward model at least as many times as the number of parameters, per iteration. The ES-MDA requires running the forward model a number of times equal to the ensemble size, for each iteration. In this case, the ES-MDA computational effort is 85% less than that required by a gradient-based method.

With the aim to further reduce the computational time, Test 1.2 was performed similarly to Test 1.1, following a pilot-point approach. The hydraulic conductivity is estimated in 266 pilot points applying the ES-MDA with an ensemble size equal to 100. The performance metrics are comparable with those obtained with the fully parameterized approach. The main features of the binary field are reproduced, but the results are not optimal. The following tests were performed taking into account the binary distribution of the sandbox field. The ES-MDA was coupled with a truncated Gaussian model to simultaneously estimate the distribution of the facies and their main hydraulic and transport parameters. ES-MDA-T was first applied following the fully parametrized approach (Test 1.3). The results reproduce well the actual field with high accuracy as well as the true parameters of each facies. This test was repeated following the pilot point approach (Test 1.4), reaching good results, but with a larger error in the reproduction of the breakthrough curves compared with Test 1.3.

Both Test 1.3 and Test 1.4 performed better than Test 1.1 and Test 1.2, suggesting that the ESMDA-T is better than the standard ES-MDA in reproducing the characteristics of a binary field. In addition, the ES-MDA-T has the advantage of being able to simultaneously estimate more properties of the aquifer. This estimation could be computationally prohibitive with the ES-MDA, as each aquifer parameters has to be estimated at each cell (or each pilot point) resulting in a huge number of parameters to be estimated. Furthermore, the estimation of different aquifer parameters for each cell can lead to equifinality problems and unreliable solutions.

Test 2.1 and Test 2.2 were performed using the experimental sandbox data using the optimal configuration obtained from the synthetic cases (Test 1.3 and Test 1.4). The ES-MDA-T achieves good results, but with lower performance than that obtained for the synthetic cases. This could be due to epistemic errors in both the experimental data and the forward model structure. The ES-MDA-T allows to reproduce the main features of the field and the estimated hydraulic and transport parameters for the two facies are reasonable and close to those expected.

The last test (Test 2.3) was performed assuming that the actual field is made up of three materials, where the third material is generated by a mixing zone at the interface between the two facies. The ES-MDA-T is applied using a simple truncated Gaussian model that ensures that the three facies occur in the same sequential order; the results are comparable with those obtained for Test 2.1.

For more complex fields, truncated plurigaussian methods can be implemented to reproduce more than two facies and different types of contacts between them. Future work will investigate this aspect by carrying out new laboratory experiments on more complex fields.

6. References

Agbalaka, Chinedu C., and Dean S. Oliver. 2008. "Application of the EnKF and Localization to Automatic History Matching of Facies Distribution and Production Data." *Mathematical Geosciences* 40 (4): 353–74. https://doi.org/10.1007/s11004-008-9155-7.

Anderson, Jeffrey L. 2007. "Exploring the Need for Localization in Ensemble Data Assimilation Using a Hierarchical Ensemble Filter." *Physica D: Nonlinear Phenomena* 230 (1–2): 99–111. https://doi.org/10.1016/j.physd.2006.02.011.

Bailey, R. T., and D. Baù. 2012. "Estimating Geostatistical Parameters and Spatially-Variable Hydraulic Conductivity within a Catchment System Using an Ensemble Smoother." *Hydrology and Earth System Sciences* 16 (2): 287–304. https://doi.org/10.5194/hess-16-287-2012.

Camporese, M., G. Cassiani, R. Deiana, and P. Salandin. 2011. "Assessment of Local Hydraulic Properties from Electrical Resistivity Tomography Monitoring of a Three-Dimensional Synthetic Tracer Test Experiment." *Water Resources Research* 47 (12). https://doi.org/10.1029/2011wr010528.

Capilla, J. E., Gómez-Hernández, J. J., and Sahuquillo, A. (1998). Stochastic simulation of transmissivity fields conditional to both transmissivity and piezometric head data—3. Application to the Culebra formation at the waste isolation pilot plan (WIPP), New Mexico, USA. Journal of Hydrology, 207(3-4), 254-269.

Chen, Xingyuan, Glenn E. Hammond, Chris J. Murray, Mark L. Rockhold, Vince R. Vermeul, and John M. Zachara. 2013. “Application of Ensemble-Based Data Assimilation Techniques for Aquifer Characterization Using Tracer Data at Hanford 300 Area: Tracer Data Assimilation at Hanford 300 Area.” *Water Resources Research* 49 (10): 7064–76. https://doi.org/10.1002/2012WR013285.

Chen, Yan, and Dean S. Oliver. 2010. “Cross-Covariances and Localization for EnKF in Multiphase Flow Data Assimilation.” *Computational Geosciences* 14 (4): 579–601. https://doi.org/10.1007/s10596-009-9174-6.

Chen, Yan, and Dongxiao Zhang. 2006. “Data Assimilation for Transient Flow in Geologic Formations via Ensemble Kalman Filter.” *Advances in Water Resources* 29 (8): 1107–22. https://doi.org/10.1016/j.advwatres.2005.09.007.

Chen, Zi, J. Jaime Gómez-Hernández, Teng Xu, and Andrea Zanini. 2018. “Joint Identification of Contaminant Source and Aquifer Geometry in a Sandbox Experiment with the Restart Ensemble Kalman Filter.” *Journal of Hydrology* 564 (September): 1074–84. https://doi.org/10.1016/j.jhydrol.2018.07.073.

Chen, Zi, Teng Xu, J. Jaime Gómez-Hernández, and Andrea Zanini. 2021. “Contaminant Spill in a Sandbox with Non-Gaussian Conductivities: Simultaneous Identification by the Restart Normal-Score Ensemble Kalman Filter.” *Mathematical Geosciences* 53 (7): 1587–1615. https://doi.org/10.1007/s11004-021-09928-y.

Chen, Zi, Teng Xu, J. Jaime Gómez-Hernández, Andrea Zanini, and Quanping Zhou. 2022. “Reconstructing the Release History of a Contaminant Source with Different Precision via the Ensemble Smoother with Multiple Data Assimilation.” *Journal of Contaminant Hydrology*, November, 104115. https://doi.org/10.1016/j.jconhyd.2022.104115.

Citarella, Donato, Fausto Cupola, Maria Giovanna Tanda, and Andrea Zanini. 2015. “Evaluation of Dispersivity Coefficients by Means of a Laboratory Image Analysis.” *Journal of Contaminant Hydrology* 172 (January): 10–23. https://doi.org/10.1016/j.jconhyd.2014.11.001.

Crestani, E., M. Camporese, D. Baú, and P. Salandin. 2013. “Ensemble Kalman Filter versus Ensemble Smoother for Assessing Hydraulic Conductivity via Tracer Test Data Assimilation.” *Hydrology and Earth System Sciences* 17 (4): 1517–31. https://doi.org/10.5194/hess-17-1517-2013.

Cupola, Fausto, Maria Giovanna Tanda, and Andrea Zanini. 2015. “Laboratory Sandbox Validation of Pollutant Source Location Methods.” *Stochastic Environmental Research and Risk Assessment* 29 (1): 169–82. https://doi.org/10.1007/s00477-014-0869-4.

D’Oria, Marco, Paolo Mignosa, Maria Giovanna Tanda, and Valeria Todaro. 2021. “Estimation of Levee Breach Discharge Hydrographs: Comparison of Inverse Approaches.” *Hydrological Sciences Journal*, December, 1–11. https://doi.org/10.1080/02626667.2021.1996580.

Emerick, Alexandre A., and Albert C. Reynolds. 2012. “History Matching Time-Lapse Seismic Data Using the Ensemble Kalman Filter with Multiple Data Assimilations.” *Computational Geosciences* 16 (3): 639–59. https://doi.org/10.1007/s10596-012-9275-5.

———. 2013. “Ensemble Smoother with Multiple Data Assimilation.” *Computers & Geosciences* 55 (June): 3–15. https://doi.org/10.1016/j.cageo.2012.03.011.

Evensen, Geir. 1994. “Sequential Data Assimilation with a Nonlinear Quasi-Geostrophic Model Using Monte Carlo Methods to Forecast Error Statistics.” *Journal of Geophysical Research* 99 (C5): 10143. https://doi.org/10.1029/94JC00572.

———. 2018. “Analysis of Iterative Ensemble Smoothers for Solving Inverse Problems.” *Comput. Geosci. 2018 223* 22 (3): 885–908. https://doi.org/10.1007/S10596-018-9731-Y.

Franssen, H.J. Hendricks, and W. Kinzelbach. 2009. “Ensemble Kalman Filtering versus Sequential Self-Calibration for Inverse Modelling of Dynamic Groundwater Flow Systems.” *Journal of Hydrology* 365 (3–4): 261–74. https://doi.org/10.1016/j.jhydrol.2008.11.033.

Franssen, H. J. W. M., and Gómez-Hernández, J. J. (2002). 3D inverse modelling of groundwater flow at a fractured site using a stochastic continuum model with multiple statistical populations. Stochastic Environmental Research and Risk Assessment, 16(2), 155-174.

Godoy, Vanessa A., Gian F. Napa-García, and J. Jaime Gómez-Hernández. 2022. “Ensemble Smoother with Multiple Data Assimilation as a Tool for Curve Fitting and Parameter Uncertainty Characterization: Example Applications to Fit Nonlinear Sorption Isotherms.” *Mathematical Geosciences* 54 (4): 807–25. https://doi.org/10.1007/s11004-021-09981-7.

Hamill, Thomas M., Jeffrey S. Whitaker, and Chris Snyder. 2001. “Distance-Dependent Filtering of Background Error Covariance Estimates in an Ensemble Kalman Filter.” *Monthly Weather Review* 129 (11): 2776–90. https://doi.org/10.1175/1520-0493(2001)129<2776:DDFOBE>2.0.CO;2.

Lam, D.-T., P. Renard, J. Straubhaar, and J. Kerrou. 2020. “Multiresolution Approach to Condition Categorical Multiple-Point Realizations to Dynamic Data With Iterative Ensemble Smoothing.” *Water Resources Research* 56 (2). https://doi.org/10.1029/2019WR025875.

Leeuwen, Peter Jan van, and Geir Evensen. 1996. “Data Assimilation and Inverse Methods in Terms of a Probabilistic Formulation.” *Monthly Weather Review* 124 (12): 2898–2913. https://doi.org/10.1175/1520-0493(1996)124<2898:DAAIMI>2.0.CO;2.

Liu, Ning, and Dean S. Oliver. 2005. “Ensemble Kalman Filter for Automatic History Matching of Geologic Facies.” *Journal of Petroleum Science and Engineering* 47 (3–4): 147–61. https://doi.org/10.1016/j.petrol.2005.03.006.

Matheron, G., H. Beucher, C. de Fouquet, A. Galli, D. Guerillot, and C. Ravenne. 1987. “Conditional Simulation of the Geometry of Fluvio-Deltaic Reservoirs.” In *All Days*, SPE-16753-MS. Dallas, Texas: SPE. https://doi.org/10.2118/16753-MS.

Todaro, Valeria, Marco D’Oria, Maria Giovanna Tanda, and J. Jaime Gómez-Hernández. 2019. “Ensemble Smoother with Multiple Data Assimilation for Reverse Flow Routing.” *Computers & Geosciences* 131 (October): 32–40. https://doi.org/10.1016/j.cageo.2019.06.002.

———. 2021. “Ensemble Smoother with Multiple Data Assimilation to Simultaneously Estimate the Source Location and the Release History of a Contaminant Spill in an Aquifer.” *Journal of Hydrology* 598 (January). https://doi.org/10.1016/j.jhydrol.2021.126215.

———. 2022. “GenES-MDA: A Generic Open-Source Software Package to Solve Inverse Problems via the Ensemble Smoother with Multiple Data Assimilation.” *Computers &amp$\mathsemicolon$ Geosciences* 167 (October): 105210. https://doi.org/10.1016/j.cageo.2022.105210.

Tong, Juxiu, Bill X. Hu, and Jinzhong Yang. 2013. “Data Assimilation Methods for Estimating a Heterogeneous Conductivity Field by Assimilating Transient Solute Transport Data via Ensemble Kalman Filter: DATA ASSIMILATION METHODS FOR TRANSIENT SOLUTE TRANSPORT MODELING.” *Hydrological Processes* 27 (26): 3873–84. https://doi.org/10.1002/hyp.9523.

Vrugt, Jasper A., Philip H. Stauffer, Th Wöhling, Bruce A. Robinson, and Velimir V. Vesselinov. 2008. “Inverse Modeling of Subsurface Flow and Transport Properties: A Review with New Developments.” *Vadose Zone Journal* 7 (2): 843–64. https://doi.org/10.2136/vzj2007.0078.

Wen, X. -H., T. T. Tran, R. A. Behrens, and J. J. Gomez-Hernandez. 2002. “Production Data Integration in Sand/Shale Reservoirs Using Sequential Self-Calibration and GeoMorphing: A Comparison.” *SPE Reservoir Evaluation & Engineering* 5 (03): 255–65. https://doi.org/10.2118/78139-PA.

Wen, X. H., Capilla, J. E., Deutsch, C. V., Gómez-Hernández, J. J., and Cullick, A. S. (1999). A program to create permeability fields that honor single-phase flow rate and pressure data. Computers & Geosciences, 25(3), 217-230.

Xu, Teng, and J. Jaime Gómez-Hernández. 2018. “Simultaneous Identification of a Contaminant Source and Hydraulic Conductivity via the Restart Normal-Score Ensemble Kalman Filter.” *Advances in Water Resources* 112 (February): 106–23. https://doi.org/10.1016/j.advwatres.2017.12.011.

Xu, Teng, J. Jaime Gómez-Hernández, Zi Chen, and Chunhui Lu. 2021. “A Comparison between ES-MDA and Restart EnKF for the Purpose of the Simultaneous Identification of a Contaminant Source and Hydraulic Conductivity.” *Journal of Hydrology* 595 (April): 125681. https://doi.org/10.1016/j.jhydrol.2020.125681.

Zhang, Yanhui, Dean S. Oliver, Yan Chen, and Hans J. Skaug. 2015. “Data Assimilation by Use of the Iterative Ensemble Smoother for 2D Facies Models.” *SPE Journal* 20 (01): 169–85. https://doi.org/10.2118/170248-PA.

Zhao, Yong, Albert C. Reynolds, and Gaoming Li. 2008. “Generating Facies Maps by Assimilating Production Data and Seismic Data with the Ensemble Kalman Filter.” In *All Days*, SPE-113990-MS. Tulsa, Oklahoma, USA: SPE. https://doi.org/10.2118/113990-MS.

Zhou, Haiyan, J. Jaime Gómez-Hernández, and Liangping Li. 2014. “Inverse Methods in Hydrogeology: Evolution and Recent Trends.” *Advances in Water Resources* 63 (January): 22–37. https://doi.org/10.1016/j.advwatres.2013.10.014.

Zimmerman, D. A., G. de Marsily, C. A. Gotway, M. G. Marietta, C. L. Axness, R. L. Beauheim, R. L. Bras, et al. 1998. “A Comparison of Seven Geostatistically Based Inverse Approaches to Estimate Transmissivities for Modeling Advective Transport by Groundwater Flow.” *Water Resources Research* 34 (6): 1373–1413. https://doi.org/10.1029/98wr00003.